Response Characteristics of the U.W. Sonic Anemometer

S. F. ZHANG

Department of Atmospheric Sciences, University of Washington, Seattle, WA 98195

J. C. WYNGAARD

National Center for Atmospheric Research, Boulder, CO 80307*

J. A. BUSINGER AND S. P. ONCLEY

Department of Atmospheric Sciences, University of Washington, Seattle, WA 98195

(Manuscript received 9 September 1985, in final form 15 November 1985)

ABSTRACT

A new sonic anemometer, called the U.W. sonic anemometer, has been designed to minimize the flow distortion due to the transducer wakes. We present a general analytical model for calculating the effect of these transducer wakes on measured velocity spectra, and show that the effects in the U.W. sonic anemometer are indeed less than in conventional arrays. We suggest a method of correcting for the errors caused by the transducer wakes.

1. Introduction

Sonic anemometers have been used extensively in atmospheric turbulence research for more than twenty years. Kaimal (1979) and Wyngaard (1981a) have done systematic reviews of its principles, response, advantages, and possible errors. One of the potentially serious but relatively unexplored sources of error is the "transducer shadow effect," or the attenuation of velocity along the acoustic paths due to the wakes of the transducers. Wyngaard and Zhang (1985) did a linearized analysis of the transducer shadow effect for the most common sonic anemometer geometry, where the horizontal velocity components are measured from a pair of axes in the horizontal plane and the vertical velocity is measured with a single vertical axis. Their analysis indicates that the effects on turbulence spectra can be quite significant.

In an attempt to minimize these wake effects, a new type of sonic anemometer (the U.W. sonic anemometer, in short) was designed by J. A. Businger and S. P. Oncley at the Department of Atmospheric Sciences, University of Washington. Figure 1 is a photograph of this unit, which also shows the mounting of thermocouples and a hot wire in the array. One can see that all six transducers and their mounting structures were taken out of the horizontal plane except for one arm needed to maintain constant separation between the transducers. The angles of the three oblique, nonorthogonal sonic paths to the horizontal are designed to be 60°, and the length of the sonic paths nominally 20 cm (Kaijo Denki Company in Japan has introduced a type of sonic anemometer–thermometer with similar probe geometry; however, their mounting structure is different from the U.W. sonic anemometer, and their three sonic paths are 45° to the horizontal). The transducers are right circular cylinders of 0.97 cm diameter and about 1.3 cm long; the transducer mounts add about 5.5 cm to the length. Other technical features of the U.W. sonic anemometer will be reported elsewhere.

Even with the new array geometry, transducer wake effects remain to be considered seriously, since small systematic errors in the measurement of the three wind components can induce large errors in the evaluation of turbulence statistics, particularly the Reynolds stress. In this paper, we present some wind tunnel calibration results for the unit, and then use these results to carry out a general linearized analysis of the transducer wake effects on turbulence spectra. We also suggest a practical method of correcting for these errors.

Flow distortion caused by the bulk of any in situ sensor can also cause significant errors in velocity measurements (Wyngaard, 1981b). This apparently has yet to be studied in detail for sonic arrays, although there are indications (e.g., Kondo and Sato, 1982) that it can be important.

* The National Center for Atmospheric Research is sponsored by the National Science Foundation.

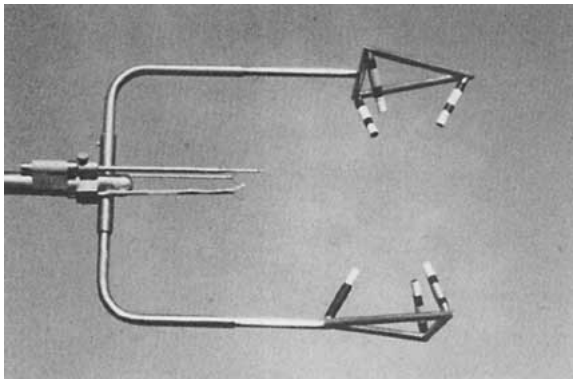

FIG. 1. Photograph of the U.W. sonic anemometer, including the mounting of the thermocouples and hot wire. Photo courtesy of R. Lind.

2. Basic relations

The basic geometry of the U.W. sonic anemometer is shown in Fig. 2. The three sonic paths are denoted by AA′, BB′, and CC′. Both the bottom triangle ABC and the top triangle A′B′C′ are designed to be equilateral. The design values of the six angles, as defined in Fig. 2, are

$$A_h = 0, \quad A_v = B_v = C_v = B_h = C_h = 60°. \quad (1)$$

The actual values of the six triangles, however, are different due to fabrication errors, as we will discuss shortly.

In coordinates aligned with the anemometer, the bottom triangle is taken as the x_1–x_2 plane, i.e., the horizontal plane: see the lower part of Fig. 2. The CB direction is designated as the x_2 axis, and the x_1 axis is to the right of the x_2 axis and perpendicular to it. The x_3 axis (vertical axis) is perpendicular to the x_1–x_2 plane and upwards. The three unit vectors along the three sonic paths, AA′, BB′, and CC′, are $\mathbf{t}_1$, $\mathbf{t}_2$, and $\mathbf{t}_3$, respectively:

$$\mathbf{t}_1 = -\cos A_h \cos A_v \mathbf{i}_1 + \sin A_h \cos A_v \mathbf{i}_2 + \sin A_v \mathbf{i}_3$$

$$\mathbf{t}_2 = \cos B_h \cos B_v \mathbf{i}_1 - \sin B_h \cos B_v \mathbf{i}_2 + \sin B_v \mathbf{i}_3$$

$$\mathbf{t}_3 = \cos C_h \cos C_v \mathbf{i}_1 + \sin C_h \cos C_v \mathbf{i}_2 + \sin C_v \mathbf{i}_3. \quad (2)$$

Here $\mathbf{i}_1$, $\mathbf{i}_2$, and $\mathbf{i}_3$ are unit vectors along the x_1, x_2, and x_3 axes, respectively.

The wind vector, $\mathbf{V}$, can be expressed by

$$\mathbf{V} = U_1\mathbf{i}_1 + U_2\mathbf{i}_2 + U_3\mathbf{i}_3, \quad (3)$$

or

$$\mathbf{V} = V(\cos\delta \cos\lambda \mathbf{i}_1 + \cos\delta \sin\lambda \mathbf{i}_2 + \sin\delta \mathbf{i}_3), \quad (4)$$

where V is the magnitude of the wind vector $\mathbf{V}$, λ is the wind direction in the horizontal plane, and δ is the vertical inclination angle of $\mathbf{V}$ with respect to the sonic anemometer; U_1, U_2 and U_3 are the components of $\mathbf{V}$ along the x_1, x_2 and x_3 axes (see Fig. 6). The wind components along the sonic paths are S_1, S_2 and S_3, respectively. Thus, we have

$$S_i = \mathbf{V} \cdot \mathbf{t}_i, \quad i = 1, 2, 3.$$

From (2) and (3)

$$S_i = \sum_j a_{ij} U_j, \quad i, j = 1, 2, 3 \quad (5)$$

where the matrix

$$a_{ij} = \begin{pmatrix} -\cos A_h \cos A_v & \sin A_h \cos A_v & \sin A_v \\ \cos B_h \cos B_v & -\sin B_h \cos B_v & \sin B_v \\ \cos C_h \cos C_v & \sin C_h \cos C_v & \sin C_v \end{pmatrix}. \quad (6)$$

On the other hand, from (5) the three wind components, U_i can be determined from the three sonic path speeds, i.e.,

$$U_i = \sum_j b_{ij} S_j, \quad i, j = 1, 2, 3 \quad (7)$$

where

$$b_{ij} = (a_{ij})^{-1} \quad (8)$$

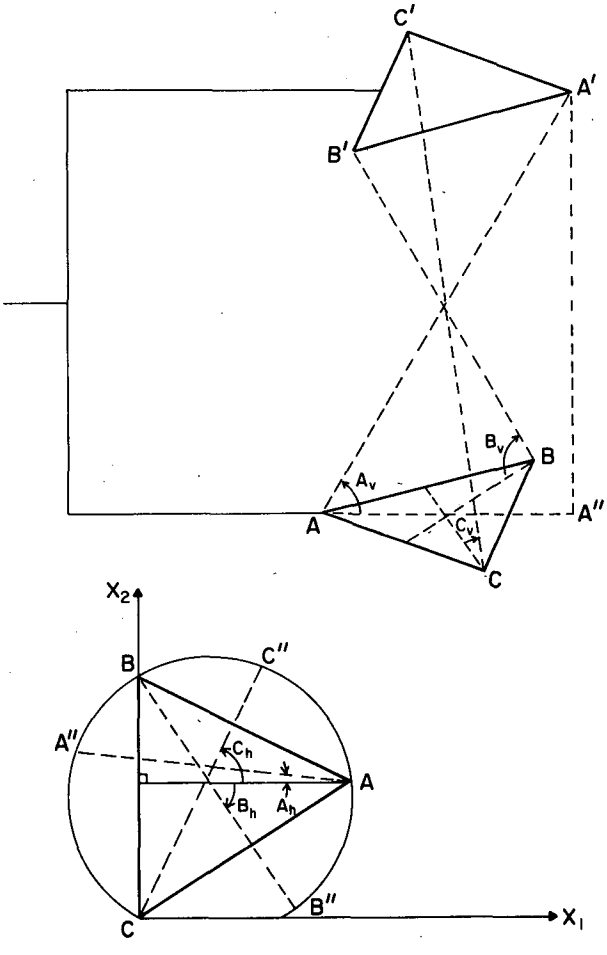

FIG. 2. Sketch of the geometry of the U.W. sonic anemometer (compare Fig. 1). The six geometric angles are defined by Eq. (10).

and

$$\sum_k a_{ik}b_{kj} = \sum_k b_{ik}a_{kj} = \delta_{ij} \tag{9}$$

where δ_{ij} is the Kronecker delta. Note that $b_{ij} \neq a_{ji}$ because $\mathbf{t}_1$, $\mathbf{t}_2$, and $\mathbf{t}_3$ are not mutually perpendicular. Mathematically, the relationship between the sonic path speeds (S_i) and the wind components (U_i) for the common sonic anemometer is a special case of (5) and (7). For example, if $A_v = B_v = C_h = 0°$, $A_h = \alpha - 180°$, $B_h = -\alpha$, and $C_v = 90°$, then (5) and (7) reduce to Eqs. (2)–(5) of Wyngaard and Zhang (1985).

For the common sonic anemometer, the "tilt errors" are well understood, and it has been suggested (Kaimal and Haugen, 1969) that an accuracy of at least ±0.1° in the internal alignment and mounting is a minimum requirement. For the U.W. sonic anemometer, it is clear from (6)–(8) that small deviations of the six angles from their design values will introduce systematic errors in the response of the anemometer. Accordingly, it is essential to determine the actual values of the six angles as accurately as possible.

In practice it is relatively easy to measure the distances between the different transducers with comparatively high accuracy. From these values of the distances, the corresponding coordinates of the six points, $A(x_1, y_1, z_1)$, $B(x_2, y_2, z_2)$, $C(x_3, y_3, z_3)$, $A'(x'_1, y'_1, z'_1)$, $B'(x'_2, y'_2, z'_2)$ and $C'(x'_3, y'_3, z'_3)$ can be determined. Then the six angles can be calculated from

$$A_h = \arctan[(y'_1 - y_1)/(x_1 - x'_1)]$$

$$A_v = \arctan\{z'_1/[(x_1 - x'_1)^2 + (y_1 - y'_1)^2]^{1/2}\}$$

$$B_h = \arctan[(y'_2 - y_2)/(x_2 - x'_2)]$$

$$B_v = \arctan\{z'_2/[(x_2 - x'_2)^2 + (y_2 - y'_2)^2]^{1/2}\}$$

$$C_h = \arctan[(y'_3 - y_3)/(x'_3 - x_3)]$$

$$C_v = \arctan\{z'_3/[(x_3 - x'_3)^2 + (y_3 - y'_3)^2]^{1/2}\}. \tag{10}$$

The results of our determination of the six angles by this method are shown in Table 1. Note that the deviations from the design values are as large as 5°. Note also that the actual angles may change over a period of time, perhaps due to unintentional, slight bending during the operation and transportation in field experiments. Hence, it is necessary to evaluate the six angles during each field experiment. In our analysis here, we will assume (unless otherwise stated) that

$$A_h = -3.72°, \quad B_h = 63.79°, \quad C_h = 64.10°$$

$$A_v = 57.83°, \quad B_v = 60.98°, \quad C_v = 61.72°. \tag{10'}$$

TABLE 1. Results of the evaluation of the six sonic geometric angles, according to Eq. (10).

Time of evaluation	27 Aug 84	2 Nov 84	4 Mar 85
A_h (deg)	−3.736	−3.941	−3.722
A_v (deg)	58.471	58.200	57.833
B_h (deg)	64.165	65.005	63.791
B_v (deg)	61.388	61.006	60.977
C_h (deg)	64.562	63.970	64.100
C_v (deg)	61.489	60.897	61.720
d_1 (AA') cm	19.119	19.136	19.220
d_2 (BB') cm	18.550	18.613	18.522
d_3 (CC') cm	18.397	18.291	18.402

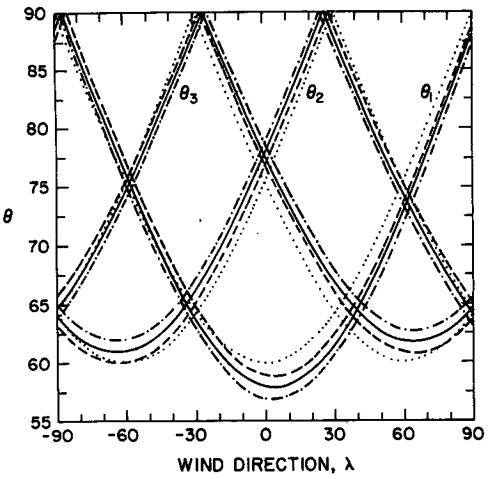

FIG. 3. Variation of the angles (θ_1, θ_2, θ_3) between the wind vector and the three sonic paths with the wind direction, see Eq. (11): $\delta = 0°$ (solid), $\delta = 1°$ (dashed), $\delta = -1°$ (dot-dashed) and $\delta = 0°$ for Eq. (1) (dotted).

The angle between the sonic paths, $\mathbf{t}_i$, and the wind vector, $\mathbf{V}$, is expressed as θ_i. From (2) and (4), it follows that

$$\theta_1 = \arccos[-\cos A_v \cos\delta \cos(A_h + \lambda) + \sin A_v \sin\delta]$$

$$\theta_2 = \arccos[\cos B_v \cos\delta \cos(B_h + \lambda) + \sin B_v \sin\delta]$$

$$\theta_3 = \arccos[\cos C_v \cos\delta \cos(C_h - \lambda) + \sin C_v \sin\delta]. \tag{11}$$

The variation of θ_i with respect to the wind direction according to (11) is illustrated in Fig. 3. One can see that the θ_i are always greater than 55°. This is distinctly different from the situation with the common array geometry, and we expect that it will give reduced transducer wake effects.

3. Wind-tunnel calibration

The three pairs of transducers in the U.W. sonic anemometer measure the wind components averaged along the three oblique sonic paths. These measured speeds, S_i^m, are generally not equal to the true speeds S_i along these sonic paths because of the effects of the transducer wakes. These effects are illustrated in Fig. 4, which shows data obtained in wind-tunnel tests at the University of California, Irvine. Figure 4 shows the variation of the wind speed along one sonic path when the angle between the wind vector and the sonic path

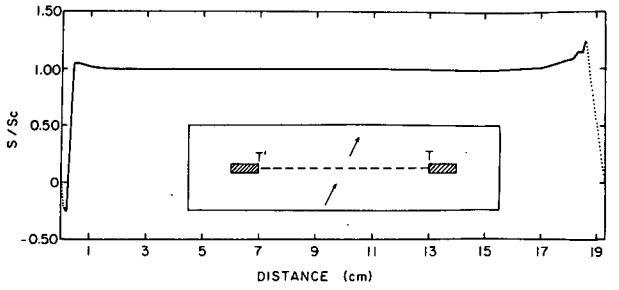

FIG. 4. The variation of the wind speed (S), normalized with the speed at the center (Sc), along a sonic path, $T'T$, (~19 cm) when the angle between the wind vector (the arrow in the inset) and the sonic path is about 60 degrees. The dotted lines represent extrapolation.

is about 60°. The wind speed has been normalized with the wind speed at the center of the 19 cm sonic path. Note that the wind speed near the transducers has significant distortion. The normalized, averaged speed along the sonic path is ~0.98.

Generally, one may assume

$$S_i^m = S_i f(\theta_i), \tag{12}$$

where f is the ratio of the measured speed to the true speed, a function of θ. Wyngaard and Zhang (1985) have shown data on f for the conventional array designs of Kaimal (1979), Hanafusa et al. (1982), and Coppin and Taylor (1983).

We attempted to establish f for the U.W. sonic anemometer through tests in the wind tunnel at the Department of Atmospheric Sciences, University of Washington (the tunnel is now located at the NOAA Western Regional Center). The cross section of the wind tunnel is 0.9 m by 1.1 m, and the size of the sonic anemometer unit is 15.2 × 29.2 × 76.2 cm; this limited the range of θ possible in the tests.

The measured speed, S_i^m, is calculated by

$$S_i^m = c^2 \Delta t_i / 2d_i, \tag{13}$$

where d_i is the length of the sonic path (see Table 1), c is the sound speed in the air, and Δt_i is the transit time difference. The sound speed in the air can be expressed as (Kaimal and Businger, 1963)

$$c = 20.067[T(1 + 0.32e/p)]^{1/2}, \tag{14}$$

where T is the air temperature, e is the water vapor pressure, and p is the atmospheric pressure. The true speed S_i is

$$S_i = V \cos(\theta_i), \tag{15}$$

where V is the air speed in the wind tunnel, and θ_i is defined by (11). During the tests T and e were measured with an Assmann psychrometer and p was deduced from weather reports. The transit time difference Δt_i was measured electronically. The value of θ was calculated from (11), by measuring λ and δ. The air speed V was measured by a standard cup anemometer, using ten minute averages; it ranged from 2–10 m s^{-1}. For each run, average values (usually 10 min) of V, T, e, p and θ were used to calculate f from (12). Averaged values of f for V in the range of 2–10 m s^{-1} are plotted against θ in Fig. 5. The large scatter in the f results in Fig. 5 can be explained as follows. From (12)–(15),

$$f(\theta) \approx \text{const} \times T\Delta t/(dV \cos\theta). \tag{16}$$

Here we ignore humidity effects, which are insignificant in this error analysis. Random errors in the measurement of T, d, V, θ, and Δt will generate a random error in $f(\theta)$. According to error theory,

$$\delta f/f = [(\delta T/T)^2 + (\delta \Delta t/\Delta t)^2 + (\delta V/V)^2 + (\delta d/d)^2 + (\tan\theta \cdot \delta\theta)^2]^{1/2}, \tag{17}$$

where δx means the standard error of x.

In our wind tunnel tests the most important factor in (17) was the last, i.e., $\tan\theta \cdot \delta\theta$ when θ is large, because we measured θ with only 0.5°–1.0° accuracy. This seems to be responsible for most of the scatter in Fig. 5, although $\delta V/V$ might be 0.5%–1.0%. Because of the possible large errors in f at large θ, we discarded the experimental data for θ greater than 80°.

Wyngaard and Zhang suggested parameterizing f by

$$f(\theta) = c + (1 - c)\sin\theta. \tag{18}$$

The curves for c = 0.90, 0.85 and 0.80 are plotted in Fig. 5. The curve for c = 0.85,

$$f(\theta) = 0.85 + 0.15 \sin\theta, \tag{19}$$

seems a plausible fit to the rather scattered data.

4. An analytical model

For the common sonic anemometer, Wyngaard and Zhang (1985) used a simple linear model to demonstrate the transducer wake effects on the spectral response. We will now extend their analysis and produce a more general model capable also of treating the more complex geometry of the U.W. sonic anemometer.

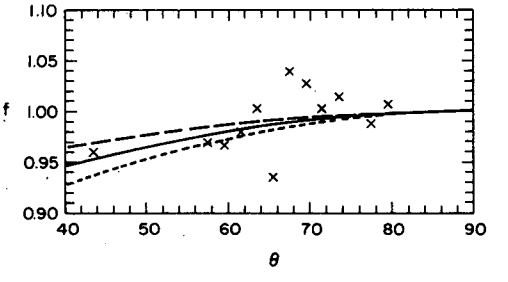

FIG. 5. The result of the wind-tunnel calibration; see Eqs. (12), (18), and (11) for the definition of f and θ. The ×'s represent experimental data. c = 0.85 (solid), c = 0.90 (long dash) and c = 0.80 (short dash).

a. Anemometer coordinates

From (5), (7) and (12), the measured wind components, U_i^m, can be written

$$U_i^m = \sum_k e_{ik} U_k, \tag{20}$$

where

$$e_{ik} = \sum_j f_j b_{ij} a_{jk}. \tag{21}$$

If the wake-effect factor $f_j = f(\theta_j) = \text{const}$, then from (9) $e_{ik} = \text{const} \times \delta_{ik}$, and from (20) $U_i^m = \text{const} \times U_i$. In the absence of flow distortion, $c = 1$, $f = 1$ and $U_i^m = U_i$.

Now, decompose the wind velocity field into mean and turbulent parts,

$$U_i = \mathbf{U}_i + u_i, \tag{22}$$

and assume $u_i/\mathbf{U}_i \ll 1$. Substitution of (22) into (20) yields:

$$u_i^m = \sum_k h_{ik} u_k, \tag{23}$$

where

$$h_{ik} = e_{ik} + (1 - c) \sum_j \cot\theta_j g_{jk} (\cos\lambda b_{ij} a_{j1} + \sin\lambda b_{ij} a_{j2} + \tan\delta b_{ij} a_{j3}) \tag{24}$$

in which e_{ik}, c and θ have been defined by (21), (18) and (11), respectively. The matrix g_{jk} has a complicated form:

$$\begin{aligned}
g_{11} &= \cos A_v \cos\delta \sin(A_h + \lambda) \sin\lambda + [\cos A_v \sin\delta \cos(A_h + \lambda) + \sin A_v \cos\delta] \cos\lambda \sin\delta \cos\delta \\
g_{12} &= -\cos A_v \cos\delta \sin(A_h + \lambda) \cos\lambda + [\cos A_v \sin\delta \cos(A_h + \lambda) + \sin A_v \cos\delta] \sin\lambda \sin\delta \cos\delta \\
g_{13} &= -[\cos A_v \sin\delta \cos(A_h + \lambda) + \sin A_v \cos\delta] \cos^2\delta \\
g_{21} &= -\cos B_v \cos\delta \sin(B_h + \lambda) \sin\lambda - [\cos B_v \sin\delta \cos(B_h + \lambda) - \sin B_v \cos\delta] \cos\lambda \sin\delta \cos\delta \\
g_{22} &= \cos B_v \cos\delta \sin(B_h + \lambda) \cos\lambda - [\cos B_v \sin\delta \cos(B_h + \lambda) - \sin B_v \cos\delta] \sin\lambda \sin\delta \cos\delta \\
g_{23} &= [\cos B_v \sin\delta \cos(B_h + \lambda) - \sin B_v \cos\delta] \cos^2\delta \\
g_{31} &= \cos C_v \cos\delta \sin(C_h - \lambda) \sin\lambda - [\cos C_v \sin\delta \cos(C_h - \lambda) - \sin C_v \cos\delta] \cos\lambda \sin\delta \cos\delta \\
g_{32} &= -\cos C_v \cos\delta \sin(C_h - \lambda) \cos\lambda - [\cos C_v \sin\delta \cos(C_h - \lambda) - \sin C_v \cos\delta] \sin\lambda \sin\delta \cos\delta \\
g_{33} &= [\cos C_v \sin\delta \cos(C_h - \lambda) - \sin C_v \cos\delta] \cos^2\delta.
\end{aligned} \tag{25}$$

The derivation of (23) is presented in the Appendix. Notice that λ and δ are now defined by the mean wind vector, i.e.,

$$\lambda = \arctan(\mathbf{U}_2/\mathbf{U}_1) \tag{26}$$

$$\delta = \arctan[\mathbf{U}_3/(\mathbf{U}_1^2 + \mathbf{U}_2^2)^{1/2}]. \tag{27}$$

The matrix h_{ik} in (24) has nine elements, which are functions of λ, δ, and the six array angles (A_h, A_v, B_h, B_v, C_h, C_v); these elements are in general nonzero. Note from (23) that each of the three measured turbulence components is a linear combination of the three true components, so there is cross talk among the turbulence components. This situation is different from that for the common sonic anemometer, where there is no cross talk between vertical and horizontal velocity components (Wyngaard and Zhang, 1985).

b. Mean-wind coordinates

Through a coordinate rotation, first with a rotation of λ [as defined by (26)] around the x_3 axis, then with a rotation of δ [as defined by (27)] around a new $\hat{x}_2$ axis (see Fig. 6), we have

$$\hat{u}_i = \sum_k p_{ik} u_k \tag{28}$$

$$u_i = \sum_k q_{ik} \hat{u}_k \tag{29}$$

where we use a caret to denote quantities measured in mean-wind coordinates. The matrices p_{ik} and q_{ik} are

$$p_{ik} = \begin{pmatrix} \cos\delta\cos\lambda & \cos\delta\sin\lambda & \sin\delta \\ -\sin\lambda & \cos\lambda & 0 \\ -\sin\delta\cos\lambda & -\sin\delta\sin\lambda & \cos\delta \end{pmatrix} \tag{30}$$

$$q_{ik} = (p_{ik})^{-1} = p_{ki} \tag{31}$$

$$\sum_j p_{ij} q_{jk} = \sum_j q_{ij} p_{jk} = \delta_{ik}. \tag{32}$$

It is easy to prove that

$$\hat{\mathbf{U}}_2 = \hat{\mathbf{U}}_3 = 0.$$

Since the transformation from sonic anemometer coordinates to the mean-wind coordinates is orthogonal, (31) holds.

From (23), (28) and (29), we have

$$\hat{u}_i^m = \sum_n r_{in} \hat{u}_n, \tag{33}$$

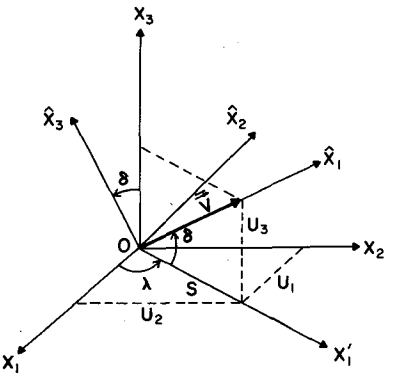

FIG. 6. The transformation from the sonic-anemometer coordinates (x_1, x_2, x_3) to the mean-wind coordinates $(\hat{x}_1, \hat{x}_2, \hat{x}_3)$. $\bar{V}$ is the mean wind vector.

where

$$r_{in} = \sum_l \sum_k p_{ik} h_{kl} q_{ln}. \tag{34}$$

Equation (33) again demonstrates the cross talk among the three turbulence components. In the special case of $\lambda = \delta = 0$, that is, when the sonic anemometer coordinates and the mean-wind coordinates coincide,

$$p_{ik} = q_{ik} = \delta_{ik}$$

and we have from (34)

$$r_{in} = h_{in}.$$

The linear model of Wyngaard and Zhang (1985) is a special case of the present model. We can prove that for the conventional array

$$h_{in} = \begin{pmatrix} c_1 & c_2 & 0 \\ d_1 & d_2 & 0 \\ 0 & 0 & 1 \end{pmatrix}$$

$$r_{in} = \begin{pmatrix} p_1 & p_2 & 0 \\ q_1 & q_2 & 0 \\ 0 & 0 & 1 \end{pmatrix},$$

where c_1, c_2, d_1, d_2, p_1, p_2, q_1 and q_2 are defined in their paper. Table 1 of that paper can be exactly reproduced by (34).

In the absence of wake effects $c = 1, f = 1$, and from (9), (21), (24), (32) and (34), $h_{ik} = e_{ik} = \delta_{ik}$, $r_{in} = \delta_{in}$ and $\hat{u}_i^m = \hat{u}_i$. This means that the three turbulence components are measured without error. In practice, the sonic anemometer is generally aligned with the prevailing wind direction, so that λ can be limited to $\pm 80°$, or an even smaller range. Since δ represents the angle between the true horizontal plane and the bottom plane of the sonic anemometer (plane ABC, Fig. 1), it is equivalent to the "tilt" of the sonic anemometer. Its effect, however, is different from the "tilt effect" discussed by Deacon (1968), Dyer et al. (1970), and Kaimal and Haugen (1969, 1971), since these authors did not consider the transducer wake effects.

c. *Transducer-wake effects on turbulence spectra*

Since the measured turbulence spectra are distorted in a very complicated way, as indicated by (33), for clarity we will discuss a relatively simple situation. Let us consider the atmospheric surface layer, where the sonic anemometer is mostly used. In the surface layer

$$\overline{u_1 u_2} = \overline{u_2 u_3} = 0. \tag{35}$$

The measured turbulence spectra then can be written as

$$\phi_1^m = r_{11}^2 \phi_1 + r_{12}^2 \phi_2 + r_{13}^2 \phi_3 + 2 r_{11} r_{13}\, \mathrm{Co}_{13}$$

$$\phi_2^m = r_{21}^2 \phi_1 + r_{22}^2 \phi_2 + r_{23}^2 \phi_3 + 2 r_{21} r_{23}\, \mathrm{Co}_{13}$$

$$\phi_3^m = r_{31}^2 \phi_1 + r_{32}^2 \phi_2 + r_{33}^2 \phi_3 + 2 r_{31} r_{33}\, \mathrm{Co}_{13}$$

$$\mathrm{Co}_{13}^m = r_{11} r_{31} \phi_1 + r_{12} r_{32} \phi_2 + r_{13} r_{33} \phi_3 + (r_{11} r_{33} + r_{13} r_{31})\, \mathrm{Co}_{13}. \tag{36}$$

Here ϕ_1, ϕ_2 and ϕ_3 are the spectra of u_1, u_2 and u_3, respectively; they integrate over all wavenumbers (or frequencies) to $\overline{u_1^2}$, $\overline{u_2^2}$, $\overline{u_3^2}$. The Co_{13} is the $\overline{u_1 u_3}$ cospectrum, its integral being $\overline{u_1 u_3} = -u_*^2$.

Surface-layer similarity theory provides guidance on the behavior of $\overline{u_1^2}$, $\overline{u_2^2}$ and $\overline{u_3^2}$ near the earth's surface. For stable and neutral conditions, Monin-Obukhov similarity theory (Busch, 1973) predicts that

$$\overline{u_1^2} = A^2(\zeta) u_*^2$$

$$\overline{u_2^2} = B^2(\zeta) u_*^2$$

$$\overline{u_3^2} = C^2(\zeta) u_*^2, \tag{37}$$

where ζ is the stability parameter z/L, with L the Obukhov length, and z the height above ground. Under unstable conditions, Wyngaard and Coté (1974) and Panofsky et al. (1977) suggest that the relevant stability parameter for $\overline{u_1^2}$ and $\overline{u_2^2}$ is z_i/L, where z_i is the convective boundary layer depth.

From (36) and (37), the ratios of measured and true spectra in the idealized surface layer are

$$\phi_1^m/\phi_1 = r_{11}^2 + (B r_{12}/A)^2 + (C r_{13}/A)^2 - 2 r_{11} r_{13}/A^2 \tag{38}$$

$$\phi_2^m/\phi_2 = (A r_{21}/B)^2 + r_{22}^2 + (C r_{23}/B)^2 - 2 r_{21} r_{23}/B^2 \tag{39}$$

$$\phi_3^m/\phi_3 = (A r_{31}/C)^2 + (B r_{32}/C)^2 + r_{33}^2 - 2 r_{31} r_{33}/C^2 \tag{40}$$

$$\mathrm{Co}_{13}^m/\mathrm{Co}_{13} = r_{11} r_{33} + r_{13} r_{31} - r_{11} r_{31} A^2 - r_{12} r_{32} B^2 - r_{13} r_{33} C^2. \tag{41}$$

According to Panofsky and Dutton (1984), the following values of A, B and C are representative:

$$A = 2.4,\ B = 1.9,\ C = 1.25,\ \text{stable and near neutral} \tag{42}$$

$A = 3.0,\ B = 3.0,\ C = 2.0,$ unstable (42′)

$A = 4.0,\ B = 4.0,\ C = 2.5,$ extremely unstable. (42″)

Our results for the stable and near-neutral surface layer are presented in Fig. 7. The outstanding finding is that the shear stress cospectrum could be either underestimated (by as much as 17%) or overestimated (by as much as 5%), depending on the wind direction. The overestimation occurs when the cross talk terms more than compensate for the attenuation of the wind speed caused by the transducer shadow effect. The spectra of u_1, u_2 and u_3 are generally underestimated by several percent, depending on wind direction. This is not as serious as in the common sonic anemometer (compare with Fig. 10 in Wyngaard and Zhang, 1985), because the angles between the wind vector and the three sonic paths of the U.W. sonic anemometer are designed to be large. The effect of δ can also be seen from Fig. 7. The additional effect of $\delta = 1°$ is less than 2.5% for Co_{13}, and less than 1% for the velocity spectra.

The dotted lines in Fig. 7 represent the response when the six array angles have the design values. The small deviations from these design values in our prototype unit slightly distort the symmetry of the response with respect to the wind direction.

The differences in the wake effects on the spectra under varying stratification of the surface layer can be seen from Fig. 8. Stratification has the strongest effect on Co_{13}. For the extremely unstable surface layer, Co_{13} could be either underestimated (by as much as 54%), or overestimated (by as much as 32%). Stratification also has significant effects on the u_1 spectral response. However, in this case the response to the stratification is in the opposite direction as for Co_{13}, since A appears as a denominator in (38). The stratification has insignificant effects on the spectra of u_2 and u_3, because the cross talk terms in (39) and (40) are generally very small. Finally, the curves with $c = 0.8$ and $c = 0.9$ in (18) for stable and near-neutral stratification are also drawn in Fig. 8 for comparison.

5. Discussion

Our model results show that the parameter c of the wake-effect function f in (18) has significant influence on the spectral response. The scatter of the wind-tunnel test data (Fig. 5), however, makes it difficult to determine f with high accuracy. Nonetheless, Fig. 5 indicates that (19) is a reasonable fit to the data, and its value $f = 0.98$ at $\theta = 60°$ is consistent with the measurements at the UCI wind tunnel (Fig. 4). Furthermore, (19) is compatible with other similar experimental data; see, for example, Fig. 6 in Wyngaard and Zhang (1985). Therefore we consider (19) as suitable for the U.W. sonic anemometer and have used it in the evaluation.

The model results, summarized in Figs. 7 and 8, give us general insight into the errors in turbulence statistics measured by the U.W. sonic anemometer. In practice, however, it is probably not advisable to correct measured statistics based on these results, since several assumptions (such as the values of A, B and C) have been made. An alternative is to obtain the time series of true turbulence components, $u_i(t)$, from the measured turbulence components, $u_i^m(t)$. This could be achieved in the following way. From (33),

$$\hat{u}_i = \sum_j c_{ij}\hat{u}_j^m, \tag{43}$$

where

$$c_{ij} = (r_{ij})^{-1}. \tag{44}$$

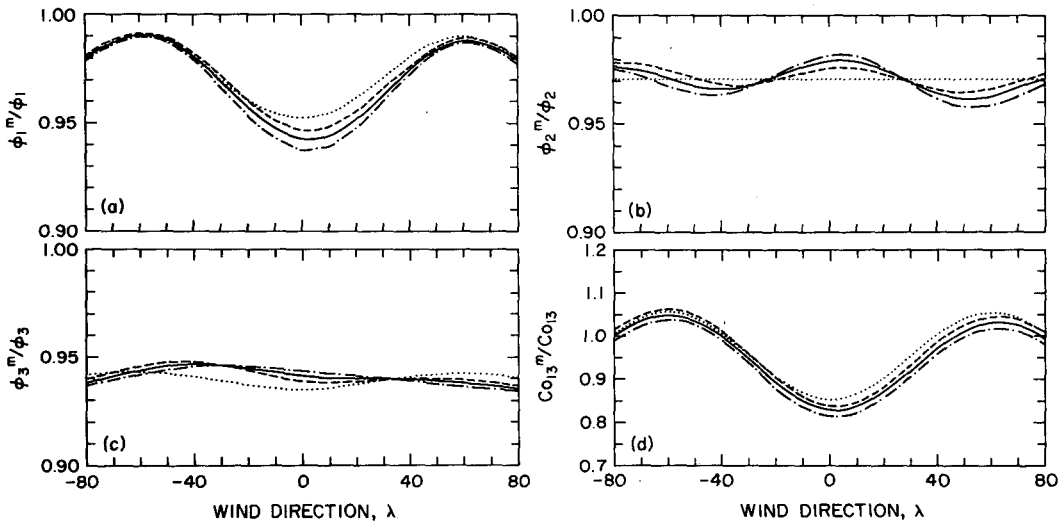

FIG. 7. Calculated spectral responses, according to (19), (38)–(42). $\delta = 0°$ (solid), $\delta = 1°$ (dashed), $\delta = -1°$ (dot-dash) and $\delta = 0°$ with Eq. (1) (dotted).

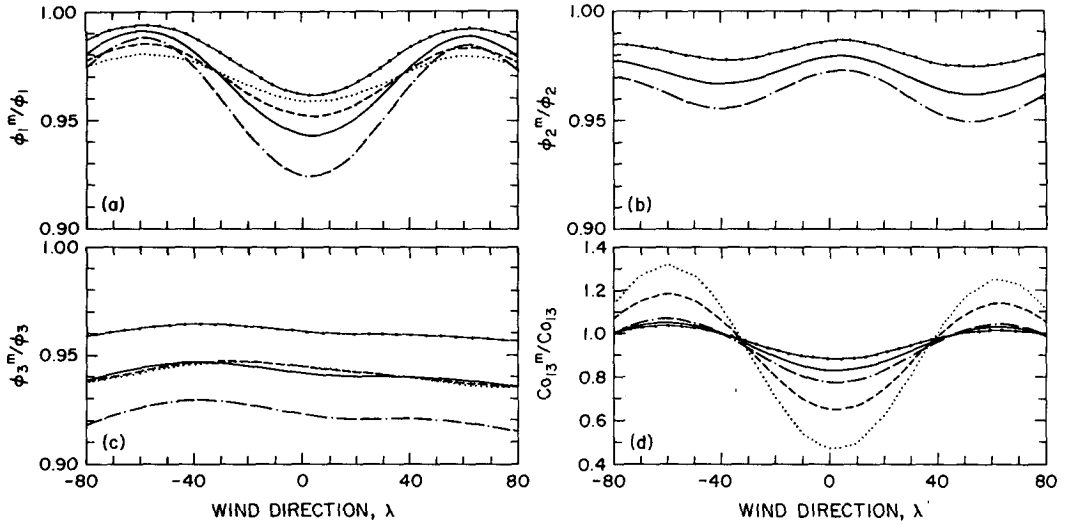

FIG. 8. Calculated spectral responses, according to (38)–(41). For (19) and (42), solid; for (19) and (42′), dashed; for (19) and (42″), dotted; $c = 0.9$ in (18) and with (42), solid with dots; and $c = 0.8$ in (18) and with (42), dot-dashed.

The matrix c_{ij} is also a function of λ, δ and the six sonic array angles. In order to evaluate c_{ij}, we have to determine the λ and δ. From (7), the time series of the three measured speeds along the three sonic paths, S_j^m, give the time series of the three measured wind components, U_i^m, i.e.,

$$U_i^m = \mathbf{U}_i^m + u_i^m = \sum_j b_{ij} S_j^m. \tag{45}$$

We can use the measured mean wind components to calculate the approximate value of λ and δ, λ^m and δ^m, by

$$\lambda^m = \arctan(\mathbf{U}_2^m/\mathbf{U}_1^m) \tag{26′}$$

$$\delta^m = \arctan[\mathbf{U}_3^m/(\mathbf{U}_1^{m2} + \mathbf{U}_2^{m2})^{1/2}]. \tag{27′}$$

Note that λ^m and δ^m are very close to λ and δ, as defined by (26) and (27); the difference is typically within 1 degree, and c_{ij} and r_{ij} vary little over that range. If higher accuracy in the values of λ and δ is needed, then an iterative method can be used. From (20),

$$U_i = \sum_j d_{ij} U_j^m, \tag{46}$$

where

$$d_{ij} = (e_{ij})^{-1} \tag{47}$$

is a function of λ and δ. We can use λ^m and δ^m as first input, then use U_i from (46) to calculate a second approximation of λ and δ, and so forth, until the desired accuracy is met.

Thus, the time series of the true turbulence components, $u_i(t)$, can be produced through the above procedure, and the evaluation of various turbulence statistics with the transducer-wake effects removed is then straightforward. As we pointed out in the Introduction, however, those "true" components are in principle subject to errors caused by the flow distortion due to the sonic array itself. Not much is yet known about these flow-distortion errors, but they can be studied experimentally by the method proposed by Wyngaard (1981b).

Acknowledgments. We are grateful to Kenneth Cumle, Department of Atmospheric Sciences, University of Washington, for the fabrication of the U.W. sonic anemometer; to John LaRue, Department of Mechanical Engineering, University of California at Irvine, for the use of their wind tunnel; to Hope Hamilton, NCAR, for skillful typing; and to Pat Waukau, NCAR, for help with programming.

Major support for this study was given by the National Science Foundation under Grant ATM8216323.

APPENDIX

Derivation of (23)

We have from the definitions in Fig. 6:

$$S^2 = U_1^2 + U_2^2 \tag{A1}$$

$$\cos\lambda = U_1/S \tag{A2}$$

$$\sin\lambda = U_2/S \tag{A3}$$

$$\tan\delta = U_3/S. \tag{A4}$$

From (A1) to (A4), it is easy to deduce:

$$d\lambda = -\sin\lambda(dU_1/S) + \cos\lambda(dU_2/S), \tag{A5}$$

$$d\delta = -\cos\lambda \sin\delta \cos\delta(dU_1/S) - \sin\lambda \sin\delta \cos\delta(dU_2/S) + \cos^2\delta(dU_3/S). \tag{A6}$$

Differentiating (11) and using (A5) and (A6) gives the following relation:

$$d(\cos\theta_1) = (dU_1/S)\{-\cos A_v \cos\delta \sin(A_h + \lambda) \sin\lambda$$
$$- [\cos A_v \sin\delta \cos(A_h + \lambda) + \sin A_v \cos\delta]$$
$$\times \cos\lambda \sin\delta \cos\delta\} + (dU_2/S)\{\cos A_v \cos\delta$$
$$\times \sin(A_h + \lambda) \cos\lambda - [\cos A_v \sin\delta \cos(A_h + \lambda)$$
$$+ \sin A_v \cos\delta] \sin\lambda \sin\delta \cos\delta\} + (dU_3/S)$$
$$\times \{[\cos A_v \sin\delta \cos(A_h + \lambda) + \sin A_v \cos\delta] \cos^2\delta\},$$

and similar relations for $d(\cos\theta_2)$ and $d(\cos\theta_3)$. In fact,

$$dU_i = u_i, \quad d\theta_i = -d(\cos\theta_i)/\sin\theta_i,$$

hence

$$d\theta_j = (S \sin\theta_j)^{-1} \sum_k g_{jk} u_k, \tag{A7}$$

where g_{ik} is expressed by (25).

On the other hand, from (20):

$$dU_i^m = \sum_k [e_{ik} u_k + \mathbf{U}_k \sum_j b_{ij} a_{jk} df(\theta_j)].$$

Incorporating with (18) and (A7), it can be written:

$$u_i^m = \sum_k \{e_{ik} + (1 - c) \sum_j \cot\theta_j [\cos\lambda b_{ij} a_{j1}$$
$$+ \sin\lambda b_{ij} a_{j2} + \tan\delta b_{ij} a_{j3}] g_{jk}\} u_k$$

or

$$u_i^m = \sum_k h_{ik} u_k,$$

which is (23).

REFERENCES

Busch, N. E., 1973: On the mechanics of atmospheric turbulence. *Workshop on Micrometeorology*, D. A. Haugen, Ed., Amer. Meteor. Soc., 1–65.

Coppin, P. A., and K. J. Taylor, 1983: A three-component sonic anemometer/thermometer system for general micrometeorological research. *Bound. Layer Meteor.*, **27**, 27–42.

Deacon, E. L., 1968: The levelling error in Reynolds stress measurement. *Bull. Amer. Meteor. Soc.*, **49**, 836.

Dyer, J. J., B. B. Hicks and V. Sitaraman, 1970: Minimizing the levelling error in Reynolds stress measurement by filtering. *J. Appl. Meteor.*, **9**, 532–534.

Hanafusa, T., T. Fujitani, Y. Kobori and Y. Mitsuta, 1982: A new type sonic anemometer-thermometer for field operation. *Pap. Meteor. Geophys.*, **33**, 1–19.

Kaimal, J. C., 1979: Sonic anemometer measurement of atmospheric turbulence. *Proc. Dynamic Flow Conf.* Skovlunde, DISA Electronic A/S, 551–565.

——, and J. A. Businger, 1963: A continuous wave sonic anemometer-thermometer. *J. Appl Meteor.*, **2**, 156–164.

——, and D. A. Haugen, 1969: Some errors in the measurement of Reynolds stress. *J. Appl. Meteor.*, **8**, 460–462.

——, and ——, 1971: Comments on "Minimizing the levelling error in Reynolds stress measurement by filtering." *J. Appl. Meteor.*, **10**, 337–339.

Kondo, J., and T. Sato, 1982: The determination of the von Karman constant. *J. Meteor. Soc. Japan*, **60**, 461–471.

Lumley, J. L., and H. A. Panofsky, 1964: *The Structure of Atmospheric Turbulence.* Interscience, 239 pp.

Panofsky, H. A., and J. A. Dutton, 1984: *Atmospheric Turbulence.* Wiley-Interscience, 397 pp.

——, H. Tennekes, D. H. Lenschow and J. C. Wyngaard, 1977: The characteristics of turbulent velocity components in the surface layer under convective conditions. *Bound. Layer Meteor.*, **11**, 355–361.

Wyngaard, J. C., 1981a: Cup, propeller, vane, and sonic anemometers in turbulence research. *Annual Reviews in Fluid Mechanics*, Vol. 13, Annual Reviews, 399–423.

——, 1981b: The effects of probe-induced flow distortion on atmospheric turbulence measurements. *J. Appl. Meteor.*, **20**, 784–794.

——, and O. R. Coté, 1974: The evolution of a convective planetary boundary layer—a higher-order-closure model study. *Bound. Layer Meteor.*, **1**, 289–308.

——, and S. F. Zhang, 1985: Transducer-shadow effects on turbulence spectra measured by sonic anemometers. *J. Atmos. Oceanic Technol.*, **2**, 548–558.